Bond Order in Two-Dimensional Metals with Antiferromagnetic Exchange Interactions

arXiv:1303.2114

Bond order in two-dimensional metals with antiferromagnetic exchange interactions

Subir Sachdev and Rolando La Placa

Department of Physics, Harvard University, Cambridge MA 02138

(Dated: July 15, 2013)

Abstract

We present an unrestricted Hartree-Fock computation of charge-ordering instabilities of two-dimensional metals with antiferromagnetic exchange interactions, allowing for arbitrary ordering wavevectors and internal wavefunctions of the particle-hole pair condensate. We find that the ordering has a dominant d symmetry of rotations about lattice points for a range of ordering wavevectors, including those observed in recent experiments at low temperatures on $YBa_2Cu_3O_y$. This d symmetry implies the charge ordering is primarily on the bonds of the Cu lattice, and we propose incommensurate bond order parameters for the underdoped cuprates. The field theory for the onset of Néel order in a metal has an emergent pseudospin symmetry which 'rotates' d-wave Cooper pairs to particle-hole pairs (Metlitski *et al.*, Phys. Rev. B **82**, 075128 (2010)): our results show that this symmetry has consequences even when the spin correlations are short-ranged and incommensurate.

A remarkable series of experiments [1–13] have shed new light on the underdoped region of the cuprate high temperature superconductors. These experiments detect a bi-directional charge density wave with a period in the range of 3 to 5 lattice spacings at low hole densities and low temperatures (T). This order is co-incident with regions of the phase diagram where quantum oscillations [14] were observed in $YBa_2Cu_3O_y$, strongly supporting the hypothesis [7, 15–18] that the charge density wave is responsible for the Fermi pockets leading to quantum oscillations. Some of the experiments [3, 5–8, 11, 12, 19, 20] also indicate that there is negligible modulation of the charge density on the Cu sites; instead, it is primarily a *bond* density wave, with modulations in spin-singlet observables on the Cu-Cu links, such as the electron kinetic energy.

This paper presents a Hartree-Fock computation of charge-ordering instabilities of a two-dimensional metal of electrons with antiferromagnetic exchange interactions (described by a 't-J' model). We allow the charge-ordering to appear at any wavevector, $\boldsymbol{Q}$, and also allow an arbitrary internal wavefunction, $\Delta_{\boldsymbol{Q}}(\boldsymbol{k})$ for the spin-singlet particle-hole pair condensate responsible for the density wave order (here $\boldsymbol{Q}$ is the center-of-mass momentum of the particle-hole pair, and $\boldsymbol{k}$ is the relative momentum). We show that this freedom leads to significant insight, despite the simplicity of our method. We find that for a range of small $\boldsymbol{Q}$ (more precisely, in the '$\mathcal{T}$ preserved' region of Fig. 2), including those observed so far in the experiments [1–6, 8–12] at low T, the dominant structure of the internal wavefunction has a d-wave form [21], with $\Delta_{\boldsymbol{Q}}(\boldsymbol{k}) \sim (\cos k_x - \cos k_y)$ for a band-structure appropriate for the cuprates. This d symmetry implies that the charge order is located primarily on the Cu-Cu links, there is little modulation of the charge density on the Cu sites, and time-reversal symmetry ($\mathcal{T}$) is preserved. We refer to this class of charge order as an 'incommensurate d-wave bond order'. Our computation also allows for other spin-singlet orders, such as Ising-nematic [22–24], 'd-density wave' [25–27], and 'circulating currents' [28], the last two of which break $\mathcal{T}$: they are all less preferred than the incommensurate d-wave bond order in the underdoped region, while Ising-nematic order is preferred at larger doping.

The preferred value of $\boldsymbol{Q}$ in our Hartree-Fock computation in a metal has the form $\boldsymbol{Q} = (\pm Q_m, \pm Q_m)$ [21]; similar orders have appeared in recent computations [21, 29, 30] using the renormalization group and other methods. At low doping, we find that $Q_m \approx Q_0$, where Q_0 is defined geometrically from the 'hot spots' on the Fermi surface, as shown in Fig. 1 (see also Fig. 3 for a comparison between the values of Q_m and Q_0). Remarkably, the hot spots of commensurate Néel order play a crucial role when the antiferromagnetic correlations are short-ranged, and even when they are incommensurate. Recent field-theoretic studies [21, 30] focused on the Fermi sur-

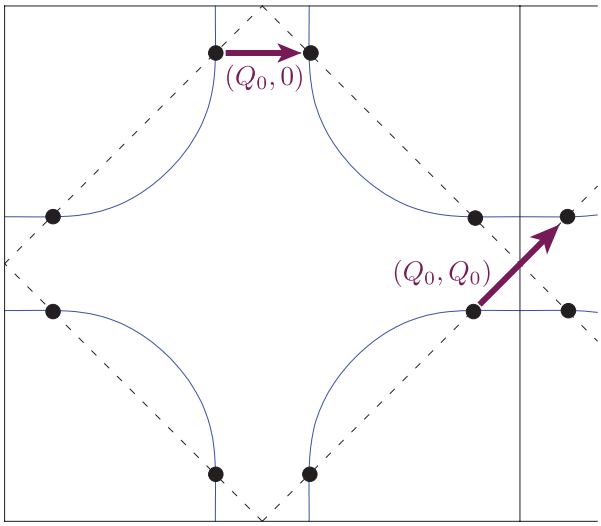

FIG. 1: Fermi surface of the hole-doped cuprates, showing the Brillouin zone boundary to antiferromagnetism at $\boldsymbol{K} = (\pi, \pi)$ (dashed lines), the hot spots (filled circles), and the wavevectors $(Q_0, 0)$ and (Q_0, Q_0).

face in the immediate vicinity of these hot spots, and this connection allows us to interpret our Hartree-Fock results in terms of an emergent approximate pseudospin symmetry [21]. The pseudospin symmetry 'rotates' d-wave Cooper pairs to particle-hole pairs: the Cooper pair amplitude $\Delta_S(\boldsymbol{k})$ rotates into $\Delta_{\boldsymbol{Q}}(\boldsymbol{k})$, which explains the predominant d symmetry of the latter. Our results show that the pseudospin symmetry is a good guide to picking optimum states in lattice computations on models with short spin correlation lengths, even though the symmetry is exact only in a continuum limit where the spin correlation length becomes very large.

As in Ref. [21, 30], we propose that the high T pseudogap is a metal with a fluctuating multi-dimensional order with both a superconducting component, $\Delta_S(\boldsymbol{k})$, and a bond order component $\Delta_{\boldsymbol{Q}}(\boldsymbol{k})$ over a range of $\boldsymbol{Q}$ around $(\pm Q_m, \pm Q_m)$. At lower T, superconductivity appears by the polarization of this order along $\Delta_S(\boldsymbol{k})$. Subsequent static charge-ordering requires computation of the non-zero $\boldsymbol{Q}$ instabilities within the superconductor. Fortunately, the latter computation has already been performed in closely related models [31, 32]: bond order modulations were found with $\boldsymbol{Q}$ along the $(1, 0), (0, 1)$ directions, as is the case in observations at low T [1–6, 8–12]. In our metallic computations, there is a 'valley' of stability from (Q_m, Q_m) to $(Q_m, 0)$ and $(0, Q_m)$, but the global minimum is at (Q_m, Q_m) (see Fig. 2); within the superconducting phase in zero magnetic field, the balance can evidently be tipped in favor of bond order near $(\pm Q_m, 0)$ and $(0, \pm Q_m)$. The choice of ordering wavevectors between $(\pm Q_m, \pm Q_m)$ and $(\pm Q_m, 0)$, $(0, \pm Q_m)$ surely depends upon

details of the Hamiltonian, the value of T, and the presence of a magnetic field, and is perhaps not accurately estimated by our present simple Hartree-Fock computation. Nevertheless, we expect the predominant d symmetry of particle-hole pair condensate, $\Delta_{\boldsymbol{Q}}(\boldsymbol{k})$, to be robust for $|\boldsymbol{Q}| \lesssim 2Q_m$, for the same reason it is robust for the particle-particle condensate, $\Delta_S(\boldsymbol{k})$, of the superconductor.

We examine the following Hamiltonian of electrons on a square lattice of sites i at positions $\boldsymbol{r}_i$ with annihilation operators $c_{i\alpha}$, where $\alpha = \uparrow, \downarrow$ is a spin label:

$$H = \sum_{i,j} \left[\left(-\mu \delta_{ij} - t_{ij} \right) c^\dagger_{i\alpha} c_{j\alpha} + \frac{1}{2} J_{ij} \vec{S}_i \cdot \vec{S}_j \right]. \tag{1}$$

Here μ is the chemical potential, t_{ij} are the electron hopping amplitudes, J_{ij} are exchange interactions, and the electron spin operator $\vec{S}_i = \frac{1}{2} c^\dagger_{i\alpha} \vec{\sigma}_{\alpha\beta} c_{i\beta}$, with $\vec{\sigma}$ the Pauli matrices. The pseudospin symmetry acts as on the Nambu spinor $\Psi_{i\alpha} = (c_{i\alpha}, \epsilon_{\alpha\beta} c^\dagger_{i\beta})$ as a SU(2) rotation V_i in Nambu space under which $\Psi_{i\alpha} \to V_i \Psi_{i\alpha}$. A key property is that $\vec{S}_i = \frac{1}{4} \Psi^\dagger_{i\alpha} \vec{\sigma}_{\alpha\beta} \Psi_{i\beta}$, and this is *invariant* under the pseudospin transformation. Consequently the exchange interaction is invariant under independent rotations V_i on each lattice site [33], and this gauge invariance was exploited in the study of spin liquid ground states of Mott insulators [27]. The pseudospin symmetry is completely broken by the t_{ij} terms in H, and so it was expected that pseudospin symmetry plays no role in metallic states, except those that are proximate to certain spin liquids [27, 34]. Here, we are interested in metallic states proximate to systems with long-range antiferromagnetism; surprisingly, it was shown in Ref. [21], that an analog of the pseudospin gauge symmetry of Refs. [33, 35] reappears in the critical theory of the antiferromagnetic quantum critical point in a conventional metal, as 4 independent global SU(2) pseudospin rotations, one for each pair of hot spots. These rotations serve to map the d-wave Cooper pairing $\Delta_S(\boldsymbol{k})$ to the d-wave bond order $\Delta_{\boldsymbol{Q}}(\boldsymbol{k})$, as is also evident in our computations below.

Note that H does not contain an explicit on-site interaction, the 'Hubbard U'. Both the Cooper pair and the bond order have small on-site components because of the d symmetry, and so U is not important in selecting the ordering instabilities. The effects of U can be accounted for by 'slave particle' methods [25, 31], and its main consequence is a renormalization of the quasiparticle dispersion. Finally, such local interactions are irrelevant in the field theory of Ref. [21].

For our charge-ordering Hartree-Fock analysis, we need the best variational estimate for the mean-field Hamiltonian

$$H_{MF} = \sum_{i,j} \left(-\mu \delta_{ij} - t_{ij} - \Delta_{ij} \right) c^\dagger_{i\alpha} c_{j\alpha} \tag{2}$$

where the non-local charge order Δ_{ij} is written as

$$\Delta_{ij} = \sum_{\boldsymbol{Q}} \left[\frac{1}{V} \sum_{\boldsymbol{k}} e^{i\boldsymbol{k}\cdot(\boldsymbol{r}_i - \boldsymbol{r}_j)} \Delta_{\boldsymbol{Q}}(\boldsymbol{k}) \right] e^{i\boldsymbol{Q}\cdot(\boldsymbol{r}_i + \boldsymbol{r}_j)/2}, \tag{3}$$

with V the system volume. This expression highlights the physical interpretation of $\Delta_{\boldsymbol{Q}}(\boldsymbol{k})$: (*i*) if $\Delta_{\boldsymbol{Q}}(\boldsymbol{k})$ is a constant independent of $\boldsymbol{k}$ (*i.e. s*-wave) then we have an ordinary site charge density wave at wavevector $\boldsymbol{Q}$ with only Δ_{ii} non-zero; (*ii*) if $\Delta_{\boldsymbol{Q}}(\boldsymbol{k}) \sim c_1 \cos k_x + c_2 \cos k_y$ (*d*- and extended *s*-wave) then we have bond order at wavevector $\boldsymbol{Q}$ with Δ_{ij} non-zero only if i and j are nearest neighbors. Also note that hermiticity requires $\Delta^*_{\boldsymbol{Q}}(\boldsymbol{k}) = \Delta_{-\boldsymbol{Q}}(\boldsymbol{k})$, and under time-reversal $\mathcal{T}$: $\Delta_{\boldsymbol{Q}}(\boldsymbol{k}) \to \Delta_{\boldsymbol{Q}}(-\boldsymbol{k})$.

All the functions $\Delta_{\boldsymbol{Q}}(\boldsymbol{k})$ are variational parameters, to be optimized by minimizing the free energy by $F \leq F_{MF} + \langle H - H_{MF} \rangle_{MF}$, where the average is over a thermal ensemble defined by H_{MF}. Here, we expand the r.h.s. in powers of $\Delta_{\boldsymbol{Q}}(\boldsymbol{k})$, and replace the inequality by an equality. To quadratic order in $\Delta_{\boldsymbol{Q}}$, we write the result in terms of hermitian functional operators on the Brillouin zone as

$$F = \sum_{\boldsymbol{k},\boldsymbol{k}',\boldsymbol{Q}} \Delta^*_{\boldsymbol{Q}}(\boldsymbol{k}) \sqrt{\Pi_{\boldsymbol{Q}}(\boldsymbol{k})} \mathcal{M}_{\boldsymbol{Q}}(\boldsymbol{k},\boldsymbol{k}') \sqrt{\Pi_{\boldsymbol{Q}}(\boldsymbol{k}')} \Delta_{\boldsymbol{Q}}(\boldsymbol{k}') + \ldots \tag{4}$$

where the kernel is

$$\mathcal{M}_{\boldsymbol{Q}}(\boldsymbol{k},\boldsymbol{k}') = \delta_{\boldsymbol{k},\boldsymbol{k}'} + \frac{3}{V} \chi_0(\boldsymbol{k} - \boldsymbol{k}') \sqrt{\Pi_{\boldsymbol{Q}}(\boldsymbol{k}) \Pi_{\boldsymbol{Q}}(\boldsymbol{k}')} \tag{5}$$

while the polarizability and susceptibility are

$$\Pi_{\boldsymbol{Q}}(\boldsymbol{k}) = \frac{f(\varepsilon(\boldsymbol{k} + \boldsymbol{Q}/2)) - f(\varepsilon(\boldsymbol{k} - \boldsymbol{Q}/2))}{\varepsilon(\boldsymbol{k} - \boldsymbol{Q}/2) - \varepsilon(\boldsymbol{k} + \boldsymbol{Q}/2)} \quad , \quad \chi_0(\boldsymbol{q}) = \frac{1}{4} \sum_j J_{ij} e^{i\boldsymbol{q}\cdot(\boldsymbol{r}_i - \boldsymbol{r}_j)}, \tag{6}$$

with $\varepsilon(\boldsymbol{k})$ the electron dispersion associated with t_{ij}, and f the Fermi function. From Eq. (4) we see that the linear charge-ordering instability of the metal occurs via condensation in the eigenmodes of the operator $\mathcal{M}_{\boldsymbol{Q}}(\boldsymbol{k},\boldsymbol{k}')$ with the lowest eigenvalues. We have chosen the specific forms of the kernel in Eq. (5) so that we need only solve the following eigenvalue problem

$$\frac{3}{V} \sum_{\boldsymbol{k}'} \sqrt{\Pi_{\boldsymbol{Q}}(\boldsymbol{k})} \chi_0(\boldsymbol{k} - \boldsymbol{k}') \sqrt{\Pi_{\boldsymbol{Q}}(\boldsymbol{k}')} \phi_{\boldsymbol{Q}}(\boldsymbol{k}') = \lambda_{\boldsymbol{Q}} \phi_{\boldsymbol{Q}}(\boldsymbol{k})$$

for the minimum eigenvalues $\lambda_{\boldsymbol{Q}}$ and corresponding eigenvectors $\phi_{\boldsymbol{Q}}(\boldsymbol{k})$, and their structure is independent of the overall strength of the interaction χ_0. The charge-order will then be $\Delta_{\boldsymbol{Q}}(\boldsymbol{k}) \propto$

$\phi_{\boldsymbol{Q}}(\boldsymbol{k})/\sqrt{\Pi_{\boldsymbol{Q}}(\boldsymbol{k})}$. Our principal numerical results below are on the $\boldsymbol{Q}$ dependence of $\lambda_{\boldsymbol{Q}}$, and on the $\boldsymbol{k}$ dependence of $\Delta_{\boldsymbol{Q}}(\boldsymbol{k})$ so obtained.

We also solved for the corresponding instability of the metal to the superconductor. In this case H_{MF} has the charge-ordering term Δ_{ij} replaced by the pairing term $-\sum_{\boldsymbol{k}} \Delta_S(\boldsymbol{k}) c_{\boldsymbol{k}\uparrow} c_{-\boldsymbol{k}\downarrow} + \text{H.c.}$, and the subsequent expressions have the replacements $\Delta_{\boldsymbol{Q}}(\boldsymbol{k}) \to \Delta_S(\boldsymbol{k})$, $\mathcal{M}_{\boldsymbol{Q}}(\boldsymbol{k},\boldsymbol{k}') \to \mathcal{M}_S(\boldsymbol{k},\boldsymbol{k}')$, $\Pi_Q(\boldsymbol{k}) \to \Pi_S(\boldsymbol{k})$, $\lambda_{\boldsymbol{Q}} \to \lambda_S$, with $\Pi_S(\boldsymbol{k}) = (1 - 2f(\varepsilon(\boldsymbol{k})))/(2\varepsilon(\boldsymbol{k}))$. In particular, the expression for the kernel $\mathcal{M}_S(\boldsymbol{k},\boldsymbol{k}')$ in terms of $\Pi_S(\boldsymbol{k})$ has a form identical to Eq. (5), a key consequence of the pseudospin symmetry of the exchange interaction. Note also that for dispersions with $\varepsilon(\boldsymbol{k}+\boldsymbol{Q}) = -\varepsilon(\boldsymbol{k})$ we have $\Pi_{\boldsymbol{Q}} = \Pi_S$ and so $\mathcal{M}_{\boldsymbol{Q}} = \mathcal{M}_S$; Ref. [21] pointed out that the dispersion obeys such a relationship close to the hot spots of a generic Fermi surface for $\boldsymbol{Q} = (\pm Q_0, \pm Q_0)$ (see Fig. 1)), and this then establishes the pseudospin rotation symmetry between Δ_S and $\Delta_{\boldsymbol{Q}}(\boldsymbol{k})$.

We assume an electronic dispersion $\varepsilon(\boldsymbol{k}) = -2t_1\left(\cos(k_x) + \cos(k_y)\right) - 4t_2\cos(k_x)\cos(k_y) - 2t_3\left(\cos(2k_x) + \cos(2k_y)\right) - \mu$ and a susceptibility $\chi_0(\boldsymbol{q})$ which is peaked near the antiferromagnetic wavevector

$$\chi_0(\boldsymbol{q}) = \sum_{\boldsymbol{K}} \frac{A}{4(\xi^{-2} + 2(2 - \cos(q_x - K_x) - \cos(q_y - K_y)))}, \tag{7}$$

where ξ is the antiferromagnetic correlation length, the sum extends over $\boldsymbol{K} = \pm(\pi, \pi(1-\delta)), \pm(\pi(1-\delta), \pi)$, and we used both the commensurate case $\delta = 0$ and the incommensurate case $\delta = 1/4$, with little difference between the results. We only need a short spin correlation length, ξ, and indeed obtained very similar results even for the case where $\chi_0(\boldsymbol{q})$ was obtained from Eq. (6) with only a nearest-neighbor J_{ij}. We diagonalized the kernels after discretizing the Brillouin zone to L^2 points with L up to 80, and the results below are for $t_1 = 1$, $t_2 = -0.32$, and $t_3 = 0.128$ for a range of values of T, μ, and ξ.

Numerical results. For the full range of parameters examined, we consistently found that λ_S was the minimal eigenvalue (indeed, BCS theory implies $-\lambda_S$ diverges logarithmically as $T \to 0$), and the corresponding eigenvector $\Delta_S(\boldsymbol{k})$ was well approximated by the d-wave form $\sim (\cos k_x - \cos k_y)$ (see Table I). So d-wave superconductivity is the primary instability.

For the charge ordering instabilities, we show the $\boldsymbol{Q}$ dependence of $\lambda_{\boldsymbol{Q}}$ in Figs 2 and in the supplement. We characterize the corresponding eigenvectors $\Delta_{S,\boldsymbol{Q}}(\boldsymbol{k})$ using orthonormal basis functions, $\psi_\gamma(\boldsymbol{k})$ of the square lattice space group:

$$\Delta_{\boldsymbol{Q}}(\boldsymbol{k}) = \sum_\gamma c_{\boldsymbol{Q},\gamma}\, \psi_\gamma(\boldsymbol{k}) \tag{8}$$

where $c_{\boldsymbol{Q},\gamma}$ are numerical coefficients collected in Table I. Depending upon the symmetry of $\boldsymbol{Q}$

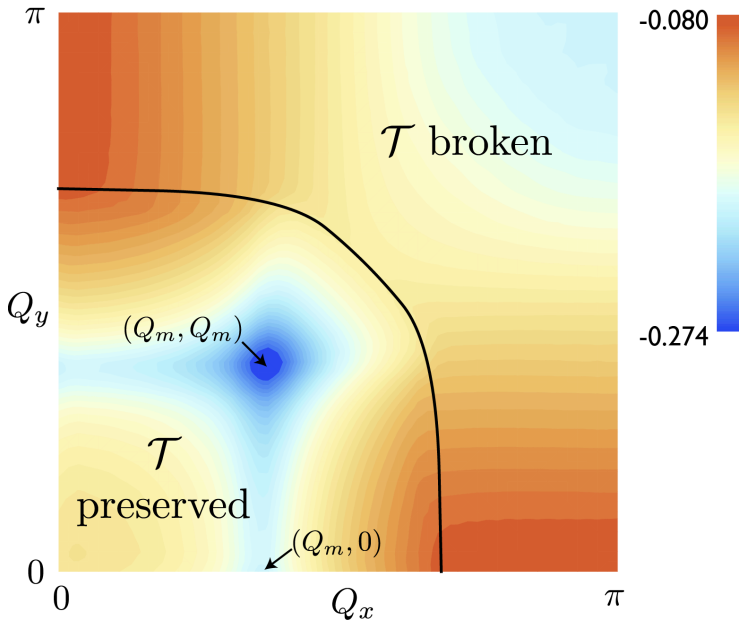

FIG. 2: Plot of $\lambda_{\boldsymbol{Q}}/A$, where $\lambda_{\boldsymbol{Q}}$ is the smallest charge order eigenvalue, as a function of Q_x and Q_y. We used $\mu = -1.11856$, $\xi = 2$, $T = 0.06$, $\delta = 1/4$ and $L = 64$. Charge order appears when $\lambda_{\boldsymbol{Q}} < -1$, which happens when A is large enough. The global minimum is at (Q_m, Q_m) and Q_m is plotted in Fig. 3 as a function of μ. Notice also the blue valleys extending from (Q_m, Q_m) to $(Q_m, 0)$ and $(0, Q_m)$. The region with time-reversal, $\mathcal{T}$, preserved has the eigenfunctions $\Delta_{\boldsymbol{Q}}(-\boldsymbol{k}) = \Delta_{\boldsymbol{Q}}(\boldsymbol{k})$ which are predominantly d, while the region with $\mathcal{T}$ broken has $\Delta_{\boldsymbol{Q}}(-\boldsymbol{k}) = -\Delta_{\boldsymbol{Q}}(\boldsymbol{k})$, as shown for some values of $\boldsymbol{Q}$ in Table I.

(in particular, the little group of the wavevector $\boldsymbol{Q}$) and of the eigenvector, some of the $c_{\boldsymbol{Q},\gamma}$ may be exactly zero. But for a generic $\boldsymbol{Q}$, only time-reversal constrains the values of $c_{\boldsymbol{Q},\gamma}$, and we are allowed to have an admixture of many basis functions. Nevertheless, only a small number of basis functions have appreciable coefficients, and so Eq. (8) represents a useful expansion.

The global minimum of $\lambda_{\boldsymbol{Q}}$ is at a wavevector along the diagonal with $\boldsymbol{Q} = (Q_m, Q_m)$, and we show a plot of Q_m as a function of chemical potential in Fig. 3. We also show the corresponding values of Q_0 as defined in Fig. 1; for small doping we see that $Q_m \approx Q_0$, one of our key results: the pseudospin symmetry of the hot-spot theory of Ref. [21] is a good guide to determining the ordering even for models with short-range, incommensurate, antiferromagnetic spin correlations. At larger doping, after the chemical potential crosses the van-Hove singularity [29], there are no hot spots, and we find $Q_m = 0$. For $\boldsymbol{Q} = (Q_m, Q_m)$, Table I shows that $\Delta_{\boldsymbol{Q}}(\boldsymbol{k})$ is predominantly d, with a small admixture of g. For $\boldsymbol{Q} = (Q_m, 0)$, $\Delta_{\boldsymbol{Q}}$ remains predominantly d, but now has a small

γ	$\psi_\gamma(\boldsymbol{k})$	$\boldsymbol{Q}$ = (Q_m, Q_m)	$\boldsymbol{Q}$ = $(Q_m, 0)$	$\boldsymbol{Q}$ = $(0,0)$	$\boldsymbol{Q}$ = (π,π)	$\Delta_S(\boldsymbol{k})$
s	1	0	-0.226	0	0	0
s'	$\cos k_x + \cos k_y$	0	0.040	0	0	0
s''	$\cos(2k_x) + \cos(2k_y)$	0	-0.051	0	0	0
d	$\cos k_x - \cos k_y$	0.993	0.964	0.997	0	0.998
d'	$\cos(2k_x) - \cos(2k_y)$	- 0.058	-0.057	-0.044	0	-0.047
d_{xy}	$2 \sin k_x \sin k_y$	0	0	0	0	0
p_x	$\sqrt{2} \sin k_x$	0	0	0	0.706	0
p_y	$\sqrt{2} \sin k_y$	0	0	0	-0.706	0
g	$(\cos k_x - \cos k_y)$ $\times \sqrt{8} \sin k_x \sin k_y$	-0.010	0	0	0	0

TABLE I: Values of $c_{\boldsymbol{Q},\gamma}$ in the expansion for $\Delta_{\boldsymbol{Q}}(\boldsymbol{k})$ in Eq. (8) for various values $\boldsymbol{Q}$ and γ. The values of $c_{\boldsymbol{Q},\gamma}$ are normalized so that $\sum_\gamma |c_{\boldsymbol{Q},\gamma}|^2 = 1$, where the sum over γ includes the small contributions from higher order basis functions not shown above. Values shown as 0 are constrained to be exactly zero by symmetry. The last column shows the coefficients in the corresponding expansion for $\Delta_S(\boldsymbol{k})$. Parameters are as in Fig. 2, and $Q_m = 4\pi/11$.

s component [32].

At $\boldsymbol{Q} = 0$, we find that $\Delta_{\boldsymbol{Q}}(\boldsymbol{k})$ is purely d: this corresponds to Ising-nematic order [22–24]. The $\mathcal{T}$-breaking 'circulating-current' order of Ref. [28] has a $p_{x,y}$ form for $\Delta_{\boldsymbol{Q}}(k)$ at $\boldsymbol{Q} = 0$, but this does not appear as a lowest eigenvalue, and so is not present in Fig. 2. Finally, $\lambda_{\boldsymbol{Q}}$ also has a broad local minimum at $\boldsymbol{Q} = (\pi, \pi)$: here $\Delta_{\boldsymbol{Q}}(\boldsymbol{k})$ does have the $p_{x,y}$ form which breaks $\mathcal{T}$, and leads to the state with spontaneous orbital currents [25–27].

Experiments [1–6, 8–12] have observed charge ordering at $\boldsymbol{Q} = (Q_m, 0), (0, Q_m)$ at low T. Choosing the largest 2 components at this wavevector from Table I, we have

$$\Delta_{\boldsymbol{Q}}(\boldsymbol{k}) = \begin{cases} \Delta_s + \Delta_d(\cos k_x - \cos k_y) & , \quad \boldsymbol{Q} = (\pm Q_m, 0) \\ \Delta_s - \Delta_d(\cos k_x - \cos k_y) & , \quad \boldsymbol{Q} = (0, \pm Q_m) \end{cases} \tag{9}$$

with $\Delta_s/\Delta_d = -0.234$. Similarly, we can have bond-ordering along $\boldsymbol{Q} = (\pm Q_m, \pm Q_m)$ with only Δ_d non-zero. We present implications of these orders for X-ray scattering, nuclear magnetic resonance, photoemission and scanning tunneling microscopy in the supplement.

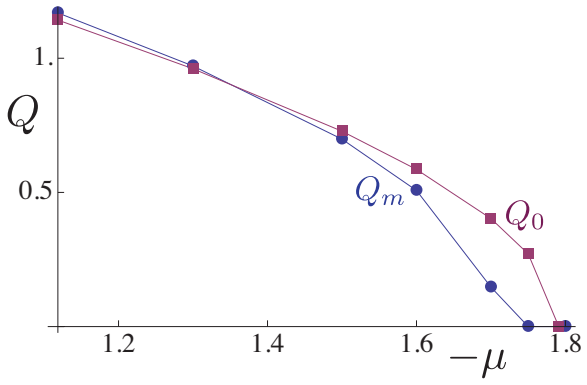

FIG. 3: Plot of Q_m (circles), where the minimum of $\lambda_{\boldsymbol{Q}}$ occurs at $\boldsymbol{Q} = (\pm Q_m, \pm Q_m)$. Also shown are the corresponding values of Q_0 (squares), as defined by the hotspots on the Fermi surface in Fig. 1. The near equality of Q_m and Q_0 is evidence for the pseudospin symmetry; note that this holds even though $\chi_0(\boldsymbol{q})$ in Eq. (7) is peaked at the wavevectors $\boldsymbol{K} = (\pi, \pm 3\pi/4), (\pm 3\pi/4, \pi)$, as is the case in many hole-doped cuprates.

Our evidence for pseudospin symmetry between Cooper pairing and charge order should have significant implications for the dynamics of these orders, which have been studied recently in Ref. [36]. For the phase diagram of the hole-doped cuprates, our model has a $T = 0$ quantum-critical point near optimal doping associated with disappearance of this bond order [7, 31]. An important challenge is to use such a critical point to describe the evolution of the Fermi surface [17], and the 'strange' metal.

Acknowledgments. We thank for A. Chubukov, D. Chowdhury, J. C. Davis, E. Demler, K. Efetov, D. Hawthorn, P. Hirschfeld, J. Hoffman, M.-H. Julien, E.-A. Kim, S. Kivelson, G. Kotliar, M.-H. Julien, H. Meier, W. Metzner, C. Pépin, C. Proust, S. Sebastian, L. Taillefer, and M. Vojta for useful discussions. This research was supported by the NSF under Grant DMR-1103860, the U.S. Army Research Office Award W911NF-12-1-0227, and the John Templeton Foundation.

[1] J. E. Hoffman *et al.*, Science **295**, 466 (2002).

[2] M. Vershinin, S. Misra, S. Ono, Y. Abe, Yoichi Ando, and A. Yazdani, Science **303**, 1995 (2004).

[3] Y. Kohsaka, *et al.*, Science **315**, 1380 (2007).

[4] W. D. Wise *et al.* Nature Physics **4**, 696 (2008).

[5] M. J. Lawler *et al.*, Nature **466**, 347 (2010).

[6] A. Mesaros *et al.*, Science **333**, 426 (2011).

[7] T. Wu *et al.*, Nature **477**, 191 (2011).

[8] Y. Kohsaka, *et al.*, Nature Physics **8**, 534 (2012).

[9] G. Ghiringhelli *et al.*, Science **337**, 821 (2012).

[10] J. Chang *et al.*, Nature Phys. **8**, 871 (2012).

[11] A. J. Achkar *et al.*, Phys. Rev. Lett. **109**, 167001 (2012).

[12] A. J. Achkar *et al.*, Phys. Rev. Lett. **110**, 017001 (2013).

[13] D. LeBoeuf, S. Krämer, W. N. Hardy, Ruixing Liang, D. A. Bonn, and C. Proust, Nature Physics **9**, 79 (2013).

[14] N. Doiron-Leyraud *et al.*, Nature **447**, 565 (2007).

[15] L. Taillefer, J. Phys.: Condens. Matter **21**, 164212 (2009).

[16] N. Harrison and S. E. Sebastian, Phys. Rev. Lett. **106**, 226402 (2011).

[17] S. E. Sebastian, N. Harrison and G. G. Lonzarich, Rep. Prog. Phys. **75**, 102501 (2012).

[18] B. Vignolle, D. Vignolles, M.-H. Julien, and C. Proust, C. R. Physique **14**, 39 (2013).

[19] K. Park and S. Sachdev, Phys. Rev. B **64**, 184510 (2001).

[20] D. Podolsky, E. Demler, K. Damle, and B. I. Halperin, Phys. Rev. B **67**, 094514 (2003).

[21] M. A. Metlitski and S. Sachdev, Phys. Rev. B **82**, 075128 (2010); New J. Phys. **12**, 105007 (2010).

[22] S. A. Kivelson, E. Fradkin, and V. J. Emery, Nature **393**, 550 (1998).

[23] H. Yamase and H. Kohno, J. Phys. Soc. Jpn. **69**, 2151 (2000).

[24] C. J. Halboth and W. Metzner, Phys. Rev. Lett. **85**, 5162 (2000).

[25] Z. Wang, G. Kotliar, and X.-F. Wang, Phys. Rev. B **42**, 8690 (1990).

[26] S. Chakravarty, R. B. Laughlin, D. K. Morr, and C. Nayak, Phys. Rev. B **63**, 094503 (2001).

[27] P. A. Lee, N. Nagaosa, and X.-G. Wen, Rev. Mod. Phys. **78**, 17 (2006). Some of the ideas on vortex structure in the superconductor discussed in this work could be transferred to our theory, with the bond order replacing the orbital current order in the vortex core: this will be explored in future work.

[28] M. E. Simon and C. M. Varma, Phys. Rev. Lett. **89**, 247003 (2002).

[29] T. Holder and W. Metzner, Phys. Rev. B **85**, 165130 (2012); C. Husemann and W. Metzner, Phys. Rev. B **86**, 085113 (2012); M. Bejas, A. Greco, and H. Yamase, Phys. Rev. B **86**, 224509 (2012); Hae-Young Kee, C. M. Puetter, and D. Stroud, J. Phys.: Condens. Matter **25**, 202201 (2013); S. Bulut, W. A. Atkinson, and A. P. Kampf, arXiv:1305.3301; J.-X. Li, C.-Q. Wu, and D.-H. Lee, Phys. Rev. B

74, 184515 (2006).

[30] K. B. Efetov, H. Meier, and C. Pépin, Nature Physics online http://dx.doi.org/10.1038/nphys2641, arXiv:1210.3276.

[31] S. Sachdev and N. Read, Int. J. Mod. Phys. B **5**, 219 (1991) (cond-mat/0402109); M. Vojta and S. Sachdev, Phys. Rev. Lett. **83**, 3916 (1999); M. Vojta, Y. Zhang, and S. Sachdev, Phys. Rev. B **62**, 6721 (2000); M. Vojta, Phys. Rev. B **66**, 104505 (2002).

[32] M. Vojta and O. Rösch, Phys. Rev. B **77**, 094504 (2008).

[33] I. Affleck, Z. Zou, T. Hsu, and P. W. Anderson, Phys. Rev. B **38**, 745 (1988); E. Dagotto, E. Fradkin, and A. Moreo, Phys. Rev. B **38**, 2926 (1988).

[34] G. Kotliar and J. Liu, Phys. Rev. B **38**, 5142 (1988).

[35] Hae-Young Kee, Annals of Physics **325**, 1260 (2010).

[36] J. P. Hinton *et al.*, arXiv:1305.1361.

[37] A. Garg, M. Randeria, and N. Trivedi, Nature Physics **4**, 762 (2008).

SUPPLEMENTARY MATERIAL

First, we give further details on the function $\lambda_{\boldsymbol{Q}}$ in Fig. 2. In Fig. 4, we plot $\lambda_{\boldsymbol{Q}}$ along different lines in the Brillouin zone, and also indicate the regions where $\mathcal{T}$ is preserved and broken.

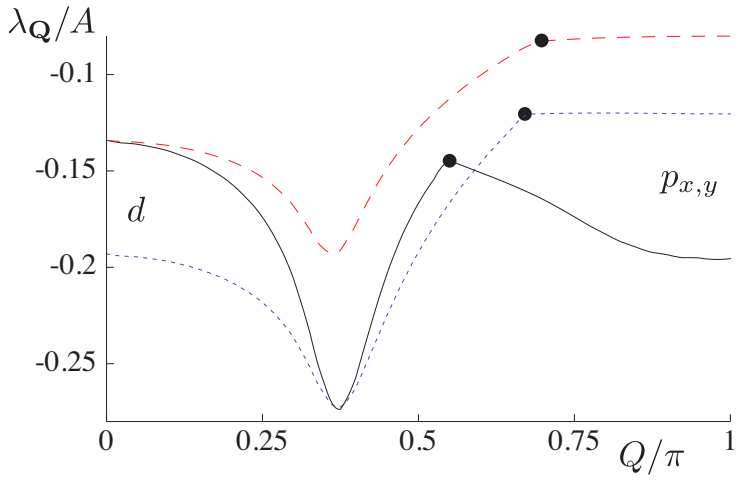

FIG. 4: Plot of the eigenvalue of Fig. 2 along the Brillouin zone diagonal with $\boldsymbol{Q} = (Q, Q)$ (full line), along the line $\boldsymbol{Q} = (Q_m, Q)$ (dotted blue line), now with $L = 80$. The eigenfunction $\Delta_{\boldsymbol{Q}}(\boldsymbol{k})$ has predominant d symmetry (as in the state of Ref. [21]) with $\mathcal{T}$ preserved to the left of the filled circles, and predominant $p_{x,y}$ symmetry with $\mathcal{T}$ broken (as in the state of Refs. [25, 26]) to the right of the filled circles. The $\boldsymbol{Q} = (0, 0)$ point corresponds to Ising nematic order [22–24].

Next, we describe properties of the bond-ordered state in Eq. (9). Inserting Eq. (9) into Eq. (3), we see that the real space order parameter Δ_{ij} is non-zero only when $i = j$, or when i and j are nearest neighbors. The values of Δ_{ii} correspond to an ordinary on-site charge density wave on the Cu sites at wavevectors $\boldsymbol{Q} = (0, \pm Q_m), (\pm Q_m, 0)$ with amplitude proportional to Δ_s. The larger component of the ordering is however the bond-density wave given by Δ_{ij} with i,j nearest neighbors, whose amplitude is proportional to Δ_d. We show plots of the values of Δ_{ij} on the bonds of the square lattice in Fig. 5 and 6. Fig 5 contains the case of uni-directional order only at the wavevectors $\boldsymbol{Q} = (\pm Q_m, 0)$, while Fig. 6 is the case of bi-directional order at wavevectors $\boldsymbol{Q} = (\pm Q_m, 0)$ and $\boldsymbol{Q} = (0, \pm Q_m)$.

For completeness, we also show the corresponding plots for ordering along $\boldsymbol{Q} = (\pm Q_m, \pm Q_m)$ in Figs 7 and 8; these appeared earlier in Figs. 22 and 23 in Ref. [21] at a different period. Note that the difference between bi-directional order at $\boldsymbol{Q} = (\pm Q_m, 0)$ and $\boldsymbol{Q} = (0, \pm Q_m)$ in Fig. 6 and bi-directional order at $\boldsymbol{Q} = \pm(Q_m, Q_m)$ and $\boldsymbol{Q} = \pm(Q_m, -Q_m)$ in Fig. 8 is subtle, and not immediately

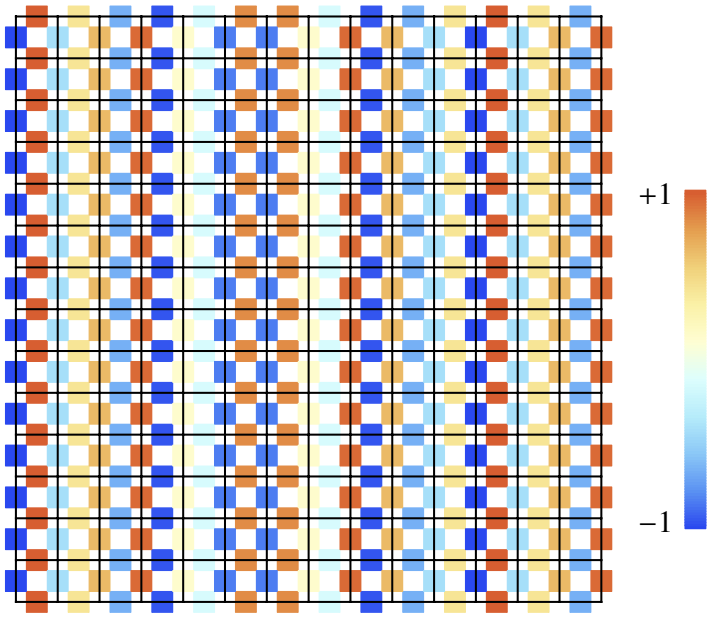

FIG. 5: Plot of the values of Δ_{ij}, when i and j are nearest neighbors; the value is denoted by a colored square centered at the midpoint between i and j. The lines intersect at the Cu sites, and the colored squares are on the O sites: the colors are therefore a measure of the charge density (or other spectral properties) on the O sites. This is also the bond-component of the ordering in Eq. (9), proportional to Δ_d; there is an additional site-component, proportional to Δ_s, which is not shown. The plot above is for the case of uni-directional order at $\boldsymbol{Q} = (\pm Q_m, 0)$ where $Q_m = 4\pi/11$, and other cases are in the following figures.

apparent at first glance: the periods along the x and y axes appear the same. However, the Fourier transforms of these two cases are distinct.

The four plots in Fig. 5-8 together contain information that should be useful in interpreting scanning tunneling microscopy, nuclear magnetic resonance, and X-ray scattering experiments: the colors can be viewed as a measure of any observable on the O site which is invariant under time-reversal and spin rotation. Most simply, such an observable is the charge density on the O site, but any spectral property of the O atom also qualifies, and the latter can have readily measurable consequences in such experiments.

Finally, we consider the electronic spectral function in the presence of bond-ordering in a metal. This is obtained by diagonalizing the following Hamiltonian

$$H_b = \sum_{\boldsymbol{k}} \left[\varepsilon(\boldsymbol{k}) c^\dagger_{\boldsymbol{k}\alpha} c_{\boldsymbol{k}\alpha} - \sum_{\boldsymbol{Q}} \Delta_{\boldsymbol{Q}}(\boldsymbol{k} + \boldsymbol{Q}/2)\, c^\dagger_{\boldsymbol{k}+\boldsymbol{Q},\alpha} c_{\boldsymbol{k}\alpha} \right], \tag{10}$$

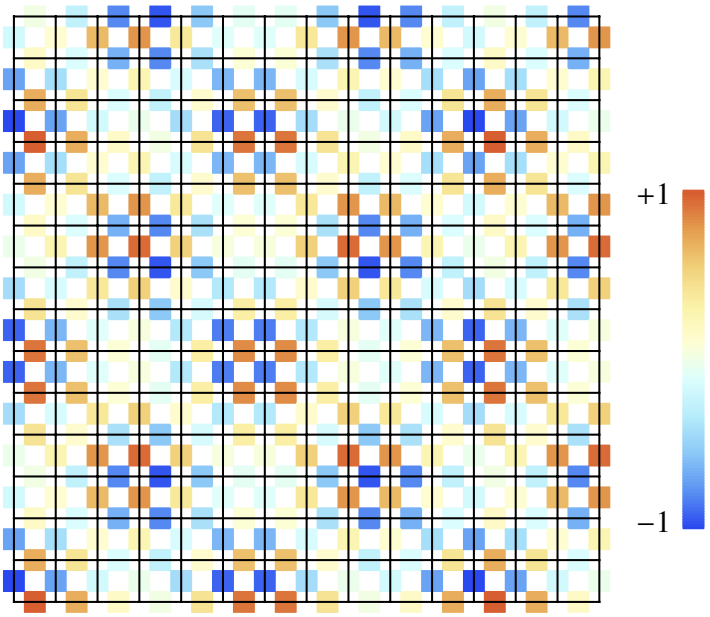

FIG. 6: As in Fig. 5, but for the case of bi-directional order at $\boldsymbol{Q} = (\pm Q_m, 0)$ and $\boldsymbol{Q} = (0, \pm Q_m)$.

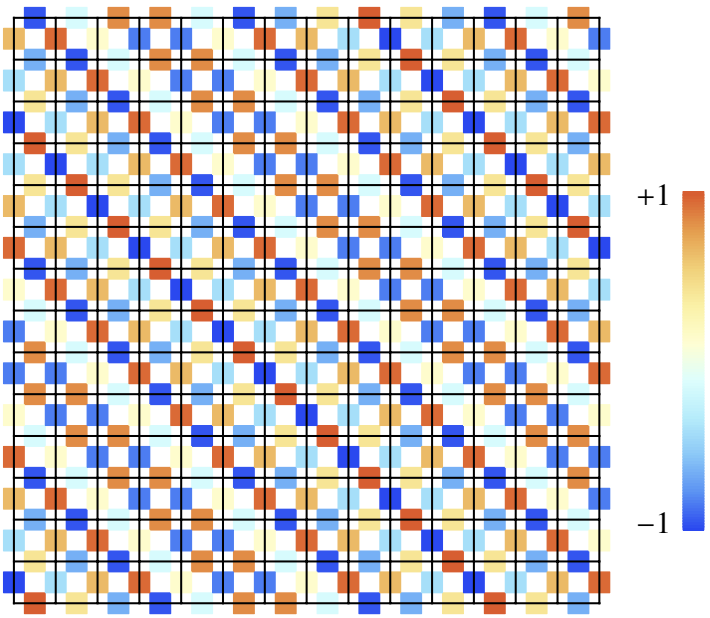

FIG. 7: As in Fig. 5, but for the case of uni-directional order at $\boldsymbol{Q} = \pm(Q_m, Q_m)$. We have chosen $\Delta_{\boldsymbol{Q}}(\boldsymbol{k})$ to be purely d, which is an excellent approximation to the state in Table I. In this case Δ_{ij} is non-zero only if i and j are nearest neighbors, and these are shown above; there is no density wave on the Cu sites. This plot also appeared in Ref. [21] with a different period.

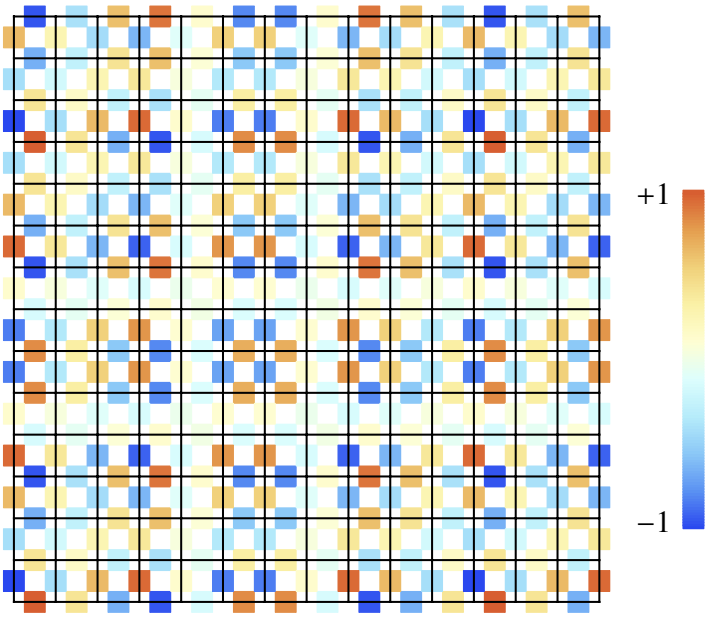

FIG. 8: As in Fig. 7, but for the case of bi-directional order at $\boldsymbol{Q} = \pm(Q_m, Q_m)$ and $\boldsymbol{Q} = \pm(Q_m, -Q_m)$.

where the sum over $\boldsymbol{k}$ extends over the complete Brillouin zone of the square lattice. For the case of bi-directional order in Eq. (9), the sum over $\boldsymbol{Q}$ extends over the 4 values $(\pm Q_m, 0)$ and $(0, \pm Q_m)$. Some care must be taken in evaluating the wavevector $\boldsymbol{Q}/2$ in the argument of $\Delta_{\boldsymbol{Q}}$ in Eq. (10) as it is not invariant under translation of $\boldsymbol{Q}$ by a reciprocal lattice vector of the square lattice: in each term, we take the momenta $\boldsymbol{k}$ and $\boldsymbol{k} + \boldsymbol{Q}$ to be separated by exactly $\boldsymbol{Q}$ (and not modulo a reciprocal lattice vector), and then $\Delta_{\boldsymbol{Q}}(\boldsymbol{k} + \boldsymbol{Q}/2)$ is evaluated at the midpoint between them. For $Q_m = 4\pi/11$, determining the spectrum of H_b involves diagonalizing a 121×121 matrix for each $\boldsymbol{k}$. From the eigenfunctions and eigenvectors we computed the imaginary part of the single-electron Green's function, $\mathrm{Im}G_{\boldsymbol{k},\boldsymbol{k}}(\omega + i\eta)$, the quantity related to the photoemission spectrum. For the bi-directional ordering along $\boldsymbol{Q} = (\pm Q_m, 0), (0, \pm Q_m)$ of Eq. (9) the result is shown in Fig. 9. The corresponding result for bi-directional ordering along $\boldsymbol{Q} = \pm(Q_m, Q_m), \pm(Q_m, -Q_m)$ is in Fig. 10; in this case $\Delta_s = 0$ by symmetry, and only Δ_d was non-zero.

The stability of the Fermi arc in the 'nodal' region ($k_x \approx k_y$) is enhanced [32, 37] because of the weak coupling to the charge order, arising from the predominant d character of Eq. (9). In the anti-nodal region, the parent Fermi surface has been gapped out by the bond order, but 'shadows' are apparent at wavevectors shifted by the charge order. However, these Fermi surfaces should be easily broadened by impurity-induced phase-shifts in the charge ordering, while protecting the

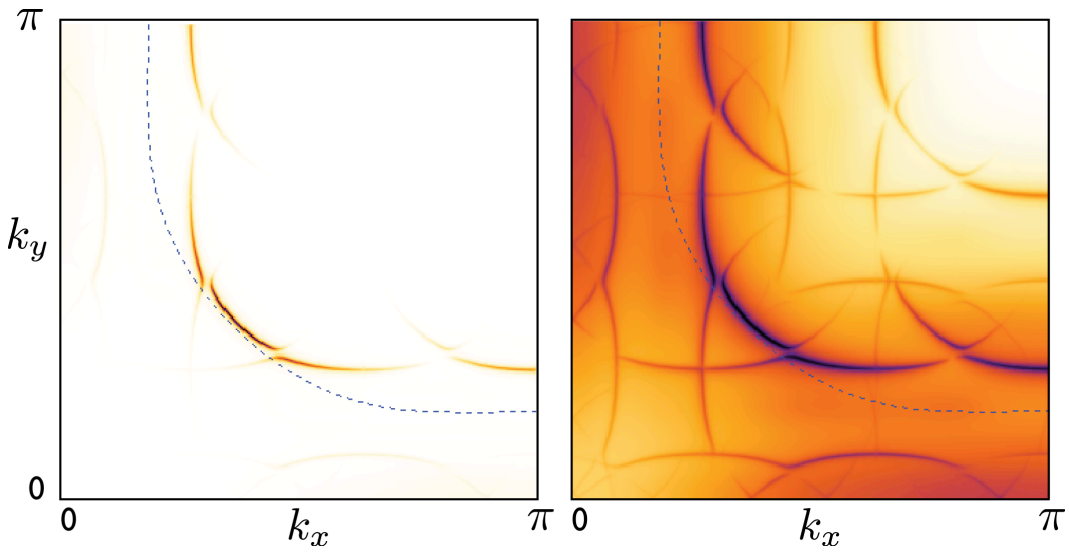

FIG. 9: Electron spectral density in the phase with bidirectional charge order at $\boldsymbol{Q} = (Q_m, 0)$ and $(0, Q_m)$ with $Q_m = 4\pi/11$. The left panel show $\mathrm{Im}G_{\boldsymbol{k},\boldsymbol{k}}(\omega + i\eta)$ at $\omega = 0$ and $\eta = 0.02$; the right panel shows $\log\left[\mathrm{Im}G_{\boldsymbol{k},\boldsymbol{k}}(\omega + i\eta)\right]$ for the same parameters, as a way of enhancing the low intensities. The dashed line is the underlying Fermi surface of the metal without charge order. The charge order is as in Eqs. (3,9) with $\Delta_d = 0.3$, $\Delta_s/\Delta_d = -0.234$, and other parameters as in Fig. 2.

nodal arcs. Furthermore, contributions from the superconducting component of the pairing order parameter should also help fully gap out the antinodal region.

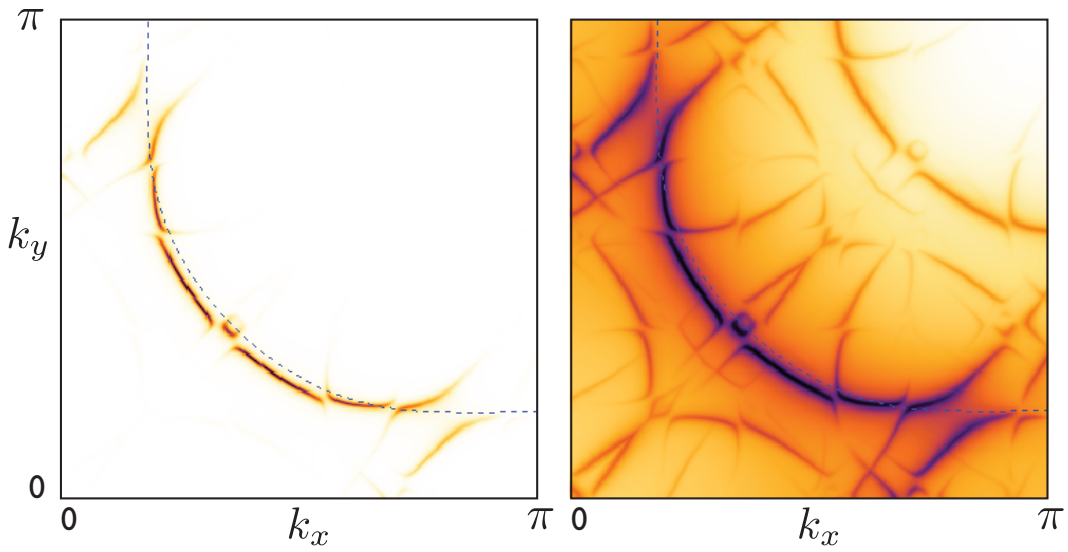

FIG. 10: As in Fig. 9, but for the case of bi-directional ordering along $\boldsymbol{Q} = \pm(Q_m, Q_m), \pm(Q_m, -Q_m)$. The charge order is as in Eqs. (3,9) with $\Delta_d = 0.3$, and $\Delta_s = 0$ is required by symmetry.